POLITECNICO DI TORINO
Repository ISTITUZIONALE

The impact of fretting wear on structural dynamics: Experiment and simulation

(Article begins on next page)

04 August 2020

Accepted Manuscript
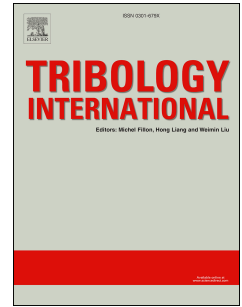
The impact of fretting wear on structural dynamics: Experiment and simulation

A. Fantetti, L.R. Tamatam, M. Volvert, I. Lawal, L. Liu, L. Salles, M.R.W. Brake, C.W. Schwingshackl, D. Nowell

The Impact of Fretting Wear on Structural Dynamics:
Experiment and Simulation

A. Fantetti[a], L. R. Tamatam[b], M. Volvert[c], I. Lawal[d], L. Liu[e], L. Salles[a], M. R. W. Brake[d],
C. W. Schwingshackl[a], D. Nowell[a]

[a]*Imperial College London, South Kensington Campus, London SW7 2AZ, UK*
[b]*Politecnico di Torino, Corso Duca degli Abruzzi 24, 10129 Torino, Italy*
[c]*Space Structures and Systems Laboratory, Department of Aerospace and Mechanical Engineering, University of Liège,
Liège, Belgium*
[d]*William Marsh Rice University, 6100 Main St., Houston, TX 77005, USA*
[e]*University of Wisconsin-Madison, 1415 Engineering Drive, Madison, WI 53706, USA*

Abstract

This paper investigates the effects of fretting wear on frictional contacts. A high frequency friction rig is used to measure the evolution of hysteresis loops, friction coefficient and tangential contact stiffness over time. This evolution of the contact parameters is linked to significant changes in natural frequencies and damping of the rig. Hysteresis loops are replicated by using a Bouc-Wen modified formulation, which includes wear to simulate the evolution of contact parameters and to model the evolving dynamic behaviour of the rig. A comparison of the measured and predicted dynamic behaviour demonstrates the feasibility of the proposed approach and highlights the need to consider wear to accurately capture the dynamic response of a system with frictional joints over its lifetime.

Keywords: Fretting Wear, Nonlinear Dynamics, Hysteresis Loops, Friction Coefficient, Contact Stiffness

1. Introduction

A major challenge in the modelling of the dynamics of jointed structures is the accurate characterization of the contact forces occurring at friction interfaces. These contact forces can lead to significant changes in natural frequencies and damping of the structure and, in addition, may lead to catastrophic failures due to the effect of wear on the single components. Several contact models have been proposed over the years to describe the contact behaviour under oscillatory loadings [1–11], with the most common model being a Coulomb slider in series with a spring (Jenkins element [5, 6]). These contact models have been successfully used in combination with harmonic balance solvers [12–16] or time integration techniques [17–19] to model the dynamics of realistic structures such as flanges [20], blades equipped with dampers or shrouds [21–25] or lap joints [17].

Due to the oscillatory nature of the excitation, frictional forces have the form of a hysteresis loop when plotted against the relative displacement that occurs between the contact interfaces (see Fig. 1.1). When a simple macroslip contact model is employed, hysteresis loops can be approximated using three contact parameters: friction coefficient, μ, normal contact stiffness, k_n, and tangential contact stiffness, k_t. These parameters are normally used as tuning factors to update numerical models, until the output of these models matches the experimental frequency response function of the assembled structure [24–27]. Some researchers have exploited instead the clear physical meaning of these contact parameters to build predictive models. In this case, an estimation of the contact parameters is performed beforehand by means of specifically designed frictional test rigs [28–30] or fully numerically by exploiting physics-based contact models where roughness is accounted for [31].

One main limitation of all the approaches above is the assumption that the contact interface does not change over time and hence the dynamic response remains unchanged. However, fretting wear will occur at the interface leading to a modification of the contact parameters and consequently of the hysteresis loop and of
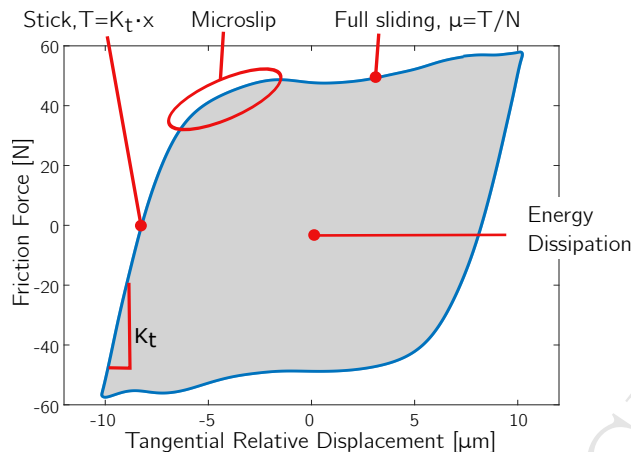
Figure 1.1: Typical hysteresis loop and its parameters: the friction coefficient μ, the contact stiffness k_t and the energy dissipation.

the dynamic response.

The goal of this work is to understand the evolution of hysteretic behavior from both a material and a structural perspective, and, in doing so, to see if new insights into the hysteretic behavior of frictional contacts can be gained. This is achieved by measuring the very high cycle evolution of hysteretic properties for fretting by using the friction rig [28] built in the Dynamics Group of Imperial College London. The test rig measures friction input parameters for industrial applications, such as the contact dynamics of aero engine components in contact. In addition, a physically based, wear evolving constitutive model is proposed to describe the hysteresis over time, and is used in combination with structural dynamics simulations to capture the evolution of the system dynamics.

2. Overview of Fretting Wear

Fretting occurs when two contacting surfaces exhibit a relative sliding motion, and is a major source of uncertainty for the dynamics modelling of jointed structures due to the lack of understanding behind it. Two types of fretting have been described in the literature [32–34]: fretting fatigue and fretting wear.

Fretting fatigue generally occurs when the relative sliding motion is small enough that part of the contact interface is stuck and part of it slips. This type of fretting involves the generation of cracks at the interface. In contrast, fretting wear occurs when the relative sliding motion is larger and the whole interface exhibits a full sliding. Fretting wear leads to the joint degradation by means of material removal. This type of fretting can also lead to noticeable system level changes in the dynamic response. Understanding the impact of fretting wear on the dynamic response of systems is crucial in designing high confidence components. In this study, the effects of fretting wear were investigated in terms of the evolution of hysteresis loops (μ and k_t) and the evolution of the system's dynamics.

2.1. Effects of fretting wear on hysteresis loops

Hysteresis loops are characterized by two contact parameters (see Fig. 1.1): friction coefficient, μ, and tangential contact stiffness, k_t. The friction coefficient defines the limit, μN, at which the contact start to slide: when the tangential force occurring between the contact interfaces equals μN the contact start to slip, where N is the normal load that pushes the interfaces together. The contact stiffness defines the stick regime of the hysteresis loop, where there is a linear relationship between the tangential force and the relative tangential displacement. This relationship is modelled as a spring with stiffness k_t (i.e. the contact stiffness), and it is due to the elastic deformation of the micro-asperities at the contact interfaces [35, 36] and to the bulk elastic deformation at the macroscopic contact scale [37–39]. In the present paper the dominant

effect is the micro-asperity deformation, as the relative tangential displacement is measured relatively close to the interfaces, less than 1mm far from the contact, making the bulk deformation effect negligible. μ and k_t are strongly affected by fretting wear:

Friction coefficient: The evolution of the friction coefficient with fretting wear has been widely investigated in the recent past [28, 40–66]. Most of those studies have confirmed that the friction coefficient rapidly increases during a running-in period, after which it reaches a steady state. The rapid increase is attributable to the removal of surface layers, such as adsorbed gas layers, oxide layers or nature pollution films, which weakens the metal-to-metal adhesion between contact interfaces [64–69]. The removal of such layers results in a metal-to-metal and/or metal-to-wear particles contact that increases the adhesive and ploughing components of the friction coefficient. When surface layers are completely removed and a balance is reached between generation and ejection of wear debris, the friction coefficient stabilizes to a steady state value [68].

Sauger et al. [70] and Fouvry et al. [71] pointed out that during the first hundred fretting cycles, a tribologically transformed surface (TTS) forms because of a plastic deformation of the metals in contact. This TTS has a nano-crystalline structure corresponding to the chemical composition of the bulk materials. This phenomenon may also be involved in the evolution during the running-in period.

Tangential Contact stiffness: To the authors' knowledge, only few studies have investigated the evolution of the tangential contact stiffness with wear [30, 41–43], since a reliable measurement of this parameter requires an accurate estimation of the relative sliding distance between specimens. In fact, in order to account for the mirco-asperity deformation only, and not for the bulk elastic deformation, the displacement measurement points need to be very close to the contact interface [54]). Schwingshackl et al. [42] measured the contact stiffness using the previous generation of the friction rig used in the present study. They found that the contact stiffness increases rapidly within the first 30,000 cycles (5 minutes at 100Hz) and then it slowly reaches a steady state in 15 minutes (corresponding to 90,000 fretting cycles) for a wide range of materials and contact conditions. This running-in is probably due to an increase in the conformity of the contact interfaces. In fact, larger areas of contact imply more asperities in contact. These asperities in contact generate more elastic deformations, which contribute to the increase in the contact stiffness.

Kartal et al. [30] also conducted fretting tests at different normal loads and observed that at low normal loads the contact stiffness remained constant with fretting cycles, while when the normal load was increased, the contact stiffness increased with the fretting cycles. This tendency of the contact stiffness to be cycle dependent at higher loads was thought to be due to the more severe fretting wear.

Lavella et al. [41] conducted experiments at higher temperatures and observed instead that the contact stiffness reaches a maximum after approximately 1 million cycles (at 100Hz and 800°C, for a Nickel alloy in a sphere-on-flat arrangement), and then decreases until reaching a steady state value close to the initial one. In a more recent study, Lavella [43] found that the contact stiffness increased within the first 500,000 fretting cycles (at 800°C) and then reached a steady state (although having a large variability that is typical of contact stiffness measurements). However, a detailed investigation focused on the evolution of the contact stiffness has not been proposed yet, and thus one of the intents of this article is to address this issue.

2.2. Effects of fretting wear on the system's dynamics

To the authors' knowledge, no experimental studies have investigated the effects of wear on the dynamic response of mechanical structures. This article aims to give insights on such effects of wear on the dynamics, and to relate those effects to their physical origins. Although there is a lack of experimental studies, more work has been conducted on numerical simulations. A great deal of research was conducted on the modelling of fretting wear for quasi-static problems as discussed, for example, in [72]. However, only few studies have attempted to model the dynamics of structures including wear over time [73–78]. Jareland and Csaba [73] included wear in a dynamic simulation of a bladed disk equipped with strip dampers, using an energy approach to estimate the worn volume at the damper interface. Salles et al. [75, 76] proposed a method for simultaneously calculating the wear and vibration response of structures. They predicted that although wear depths are very small (a few microns), these depths greatly modify the vibratory behavior of structures. Petrov [74] also investigated the effect of wear on bladed disks equipped with friction dampers. He predicted the wear generated at the contact that resulted in the loss of the fully worn out dampers. However, these

studies did not consider the evolution of the friction coefficient and the contact stiffness, which indeed were assumed constant in time.

Recently, Armand et al. [77] proposed a multiscale approach that incorporates wear into nonlinear dynamics analyses. In short, they used a semi-analytical contact solver to estimate the pressure distribution at the contact. Then, they run a state-of-the-art nonlinear dynamic analysis, which provided the system forced response and also the friction forces generated at the contact. These friction forces were used to estimate the wear volume and therefore update the contact interfaces. After the update, the semi-analytical solver was run again to predict the new pressure distribution. The process is repeated for many vibration cycles. The approach was applied to a test case of turbine blades equipped with an underplatform damper. The results of this study confirmed the sensitivity of the dynamic response to changes at the contact interface. Wear patterns strongly affect the pressure distribution, which in turn changes the slipping mechanisms occurring at the contact interfaces. In a continuation of the study, Armand et al. [78] included the roughness in the description of the contact interfaces and even predicted the evolution of contact stiffness with wear. It was found that the contact stiffness increased with wear because of an increase of the real area of contact. This stiffening of the contact interfaces also resulted in a slight increase of the system natural frequency. Their predictions are in accordance with the experimental findings of this study.

However, these studies are only preliminary attempts to model the effects of fretting wear on the dynamic forced response of jointed structures. The poor experimental knowledge restricts the ability to optimize the maintenance and design of jointed structures and it also limits our understanding of how joints deteriorate. This issue is therefore addressed in this article. Additionally, a novel formulation of wear evolution is also proposed that can be easily implemented in numerical dynamic simulations. This formulation can be applied to most of the contact models used in dynamics simulations and, in the present paper, it is applied to a Bouc-Wen model.

3. Experimental Analysis

The experiments detailed in this paper are from a fretting test rig, which was designed at Imperial College London in 2010 [28] to measure hysteresis loops for common materials used in aero engine applications. This test rig is used to measure the hysteretic properties of a contact pair, from which the friction coefficient and the tangential contact stiffness are able to be extracted as functions of energy dissipated. The experiments are conducted over a very long duration, as aero engine components experience ultra high cycle loading.

3.1. Description of the test rig

The friction rig [28] generates a flat-on-flat sliding contact between a pair of cylindrical specimens as illustrated in Fig. 3.1. The rig is composed of a moving block that slides over a static block. The moving block is excited by means of a shaker and is composed of a moving arm hinged to a larger moving mass. One specimen is clamped to the moving arm and is in contact with the other specimen that is clamped to the static block. Photo and scheme of the rig are shown in Fig. 3.2a-b. A lumped mass model of the rig was created (Fig. 3.2c) and is described in Section 4.1. The relative displacement between the sliding specimens is measured slightly above and below the contact interfaces, less than 1mm far from the contact, by means of two Laser Doppler vibrometers (LDVs). This accurate measurement method leads to a negligible effect of the bulk elastic deformation of the specimens, making the measurement of the tangential contact stiffness more reliable. The friction force is measured with dynamic load cells attached to the static block and capable to measure forces up to 10kHz. A continuous contact is ensured between the specimens by applying a normal load by means of a pneumatic actuator placed on the top of the moving block.

A typical measured hysteresis loop is shown in Fig. 1.1. The friction coefficient is obtained by dividing the friction limit (horizontal portion of the loop) by the applied normal load, and the contact stiffness is estimated from the slope of the stick portion of the loop.

Several fretting tests were conducted over different time spans in order to capture the evolution of the hysteresis loops with wear. The experimental plan and the main results are discussed in the following paragraphs.
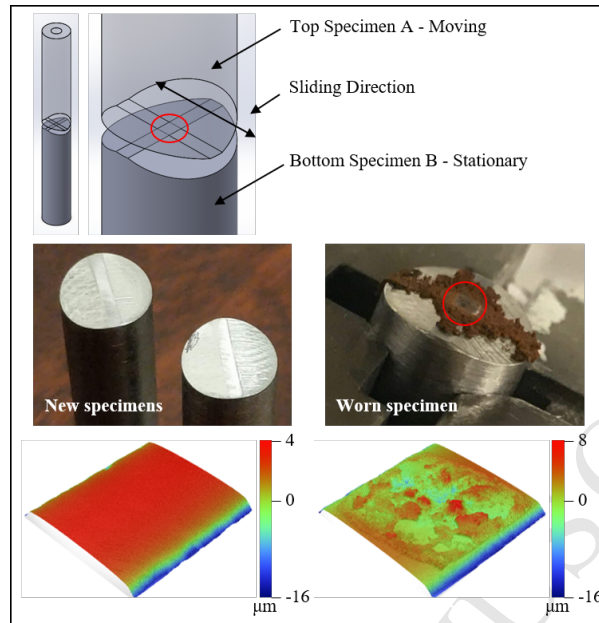
4

Figure 3.1: (Top) 3D models showing the orthogonal placement of top and bottom specimens with respect to the contact zone. (Bottom) Sample images of new and worn specimens; Scans of the contact area obtained from the optical interferometer.
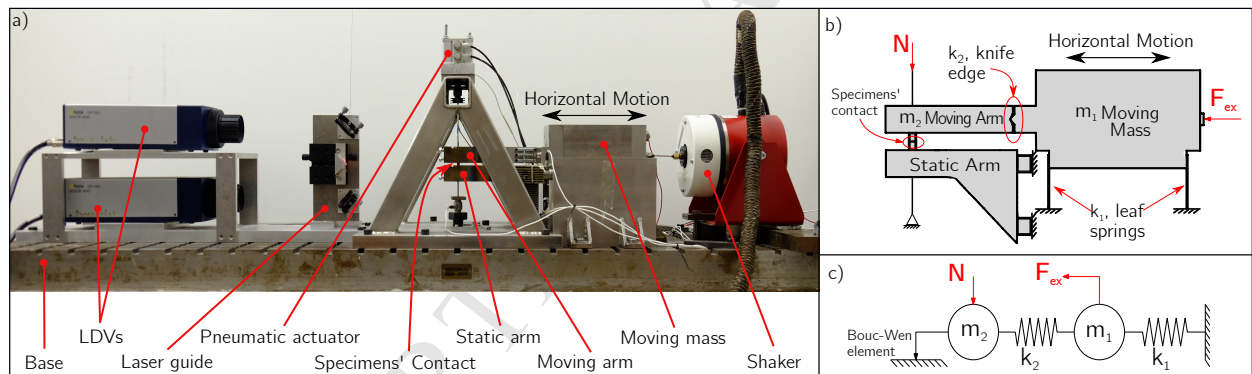

Figure 3.2: Friction rig: a) Rig's photo; b) Rig's scheme; c) Rig's two degree of freedom lumped mass model.

3.2. Wear test plan

A series of five fretting tests was conducted using different couples of specimens at room temperature. The excitation frequency was 100 Hz, which is the best working frequency for the test rig. The normal load was maintained constant at 60N for all tests. This value was chosen because it is large enough to generate hysteresis loops with the necessary amount of energy dissipated and, therefore, of fretting wear. The specimens were all made of stainless steel (SS304) and their contact interface was carefully hand polished using two different grades of sand paper: first, 800 grit for coarse and bulk material removal and then, 2500 grit for smooth and finer surface finish, leading to a roughness value R_a of about $0.1\mu m$. The width of the contact was maintained at 1mm on each specimen. In every test, the specimens were placed orthogonally as illustrated in Fig. 3.1 and for each pair the nominal area of contact was $1mm^2$ (having a 5% of variability due to the manufacturing tolerance and assembly). The resulting nominal contact pressure was therefore 60MPa.

Before and after every test, the specimens were cleaned with Iso-propyl Alcohol in an ultrasonic bath for 15 mins and, after cleaning, optical microscope images were captured using a Wyko® NT9100 optical

interferometer.

Experiments were carried out at imposed lateral force. Two tangential excitation amplitudes of 53 N and 75 N were chosen in order to investigate the effect of different strokes, on average respectively $14\mu m$ and $22\mu m$ of full relative sliding. It must be pointed out that this resulting tangential relative displacement is not imposed; it is a function of the time-dependent coefficient of friction and contact stiffness. This is clearly visible in fig. 3.3 where the relative displacement is continuously decreasing as a function of the number of cycles. Two tests were conducted at 53N excitation (average $14\mu m$ sliding) for about 5.5 hours each, and three tests were conducted at 75N excitation (average $22\mu m$ sliding) for 0.6, 3.6 and 9 hours respectively in order to assess the repeatability of the experiments. The tests specifications are summarized in Table 3.1 together with an overview of the main results.

Table 3.1: Wear tests summary.

	Units	**Test 1 / 2**	**Test 3 / 4 / 5**
Material	-	Stainless Steel	Stainless Steel
Type of Contact	-	flat-on-flat	flat-on-flat
Temperature	-	Room Temp.	Room Temp.
Contact Area	$[mm^2]$	1	1
Contact Pressure	[MPa]	60	60
Excitation Amplitude	[N]	53	73
Excitation Frequency	[Hz]	100	100
Average Sliding Distance	$[\mu m]$	$14 = \pm7$	$22 = \pm11$
Average Sliding Velocity	$[mm/s]$	2.8	4.4
Energy Dissipated/Cycle	[mJ/cycle]	$1.3 \div 1.7$	$2.0 \div 2.4$
Energy Dissipated/Sec	[mJ/s]	$130 \div 170$	$200 \div 240$
Running Time	[hrs]	5.3 / 5.5	0.6 / 3.6 / 9
Total Energy Dissipated	[J]	2800/2900	500/2900/7100
Wear Volume	$[\mu m \cdot mm^2]$	4.6 / 5.2	3.2 / 7.3 / 12.7
Friction Coefficient			
Fretting Cycles to Steady State	-	$27000 \div 30000$	$21000 \div 23600$
Energy Dissipated to Steady State	[J]	$38 \div 42$	$46 \div 52$
Steady Friction Coefficient	-	$0.89 \div 0.93$	$0.86 \div 0.88$
Contact Stiffness			
Fretting Cycles to Steady State	-	$1.8e6 \div 2.1e6$	$0.7e6 \div 1.0e6$
Energy Dissipated to Steady State	[J]	$2500 \div 3000$	$1700 \div 2250$
Steady Contact Stiffness	$[N/\mu m]$	$58 \div 67$	$46 \div 60$

3.3. Experimental Results

Three pieces of information were obtained during each test: the evolution of hysteresis loops, contact interfaces, and system dynamics. These three are described in the following paragraphs.

3.3.1. Evolution of hysteresis loops

In Fig. 3.3 the evolution of hysteresis loops over time is shown for test 1 (the trend is the same for all other tests). Both friction coefficient and contact stiffness are noticeably influenced by the wear evolution.
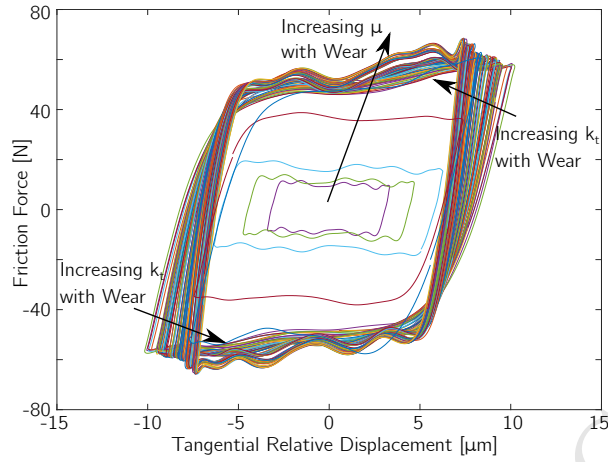
Figure 3.3: Evolution of hysteresis loops with wear for test 1: excitation frequency=100Hz, average sliding distance=$\pm7\mu m$, normal load=60N, nominal area of contact= $1mm^2$, total fretting cycles=1900000, material=Stainless Steel, temperature=25°C.
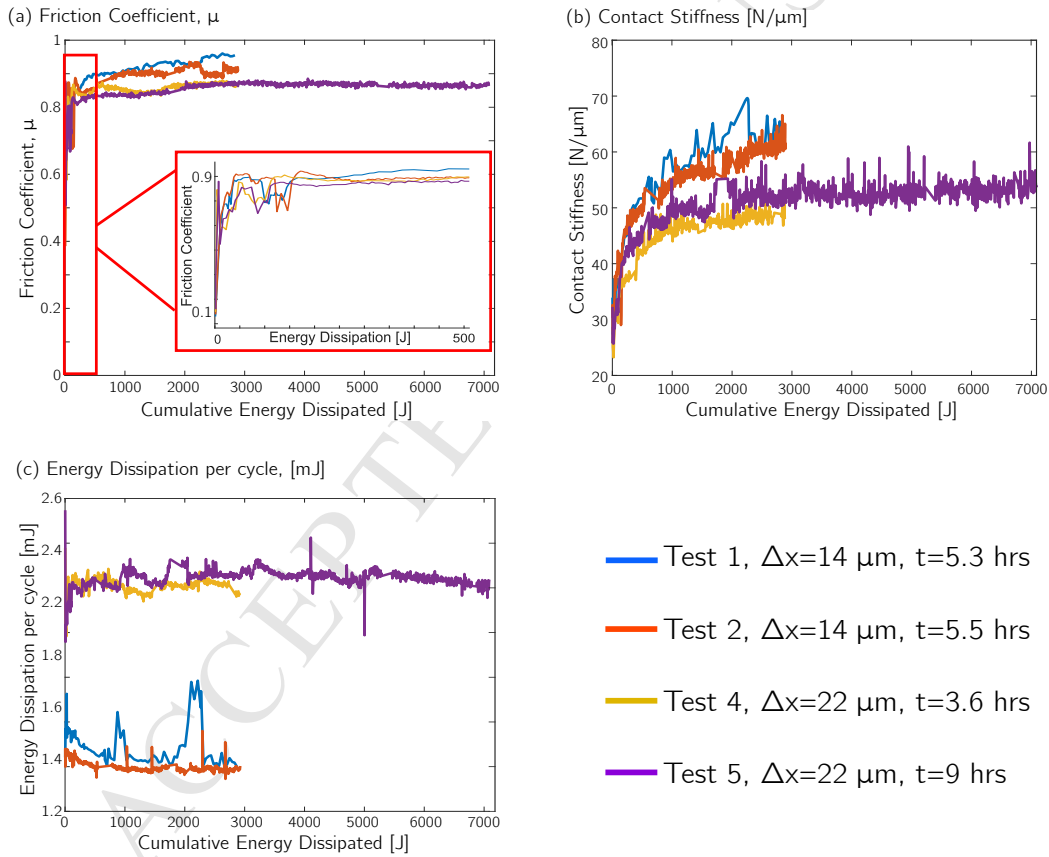
Figure 3.4: Evolution of contact parameters with wear. Test conditions: excitation frequency=100Hz, normal load=60N, nominal area of contact=$1mm^2$, material=Stainless Steel, temperature=25°C.

Friction Coefficient. The friction limit, μN, at which the contact started to slide, increased with fretting cycles. Since the normal load, N, remained constant during the whole test, this implies that the friction coefficient, μ, has increased over time as the samples became worn. The trend of the friction coefficient is

7

shown as a function of the cumulative energy dissipated in Fig 3.4a for all tests, except the test 3 that was carried out only for a short period of time. It rapidly increased by almost 9 times within the first thousands of fretting cycles from an initial value of 0.11 to a steady state value of 0.9 at room temperature. The energy dissipated was obtained as the cumulative sum of the energy dissipated within each hysteresis loop. The authors suggest plotting the evolution of the contact parameters versus the cumulative energy dissipated rather than fretting cycles, since the cumulative energy dissipated allows for a more reliable comparison of results obtained in different test conditions.

The results are repeatable because the friction coefficient maintained the same value for tests 1/2 and for tests 4/5 that were obtained for the same sliding distances. The steady state was reached after about 50J of cumulative energy dissipated for every test. The rapid increase in the coefficient of friction at the start of the tests and its convergence to a stable value agree with previously observed trends for fretting [28, 41–58, 61–66], and are further discussed in Section 3.4. The physical reason for this rapid increase in the friction coefficient has been attributed to the removal of initial oxide layers on the interfaces [64–69]. This removal results in a metal-to-metal contact and/or metal-to-wear particles contact that contribute to the increase in the friction coefficient in terms of both adhesive and ploughing components. The steady state has been attributed to a balance between the generation and ejection of wear debris from the contact [68].

Tangential Contact Stiffness. With regards to the tangential contact stiffness, fewer studies have investigated its evolution with wear [30, 41–43]. It is clear from Fig. 3.3 that the contact stiffness increases with wear as well, because the slope of the stick portion of the loops increases substantially. This increasing trend is better illustrated in Fig. 3.4b. The steady state contact stiffness has a larger variability than the steady state friction coefficient. For tests 4 and 5, it starts from an initial value of $26N/\mu m$ and it reaches a steady state at roughly $50N/\mu m$ after 2000J of cumulative energy dissipated at the contact (that is about 40 times larger than the energy required to reach a steady friction coefficient). This trend is probably due to (i) an increased conformity of the contact interfaces and also to (ii) the increased interaction between the wear scars. The increase in the interface conformity leads to a larger amount of asperities in contact, which in turn contributes to the increase in the contact stiffness. The increase in the interaction between wear scars is due to the conformity of peaks and valleys, which lock the surfaces together and add elastic resistance to the relative motion during the stick phase.

This hypothesis is supported by the evolution of the contact areas for tests 3, 4 and 5 (that where conducted for the same sliding amplitude, but different numbers of fretting cycles). In fact, as shown in Fig. 3.5, the worn area of contact is the smallest for test 3, which was run for the shortest time. In tests 4 and 5 the worn area of contact is larger, as shown by the extended wear pattern. It is assumed that larger areas of contact lead to increases in the value of the contact stiffness, since more asperities and/or wear scars are in contact, resulting in a higher number of elastic deformations. The tangential contact stiffness partly originates in fact from elastic deformations of asperities that deform under tangential loads [35, 36]. These results are in line with the numerical predictions of Armand et al. [78], who run a dynamic analysis including wear evolution. They also predicted an increase of the contact stiffness within the first fretting cycles until a steady state was attained. The observed increase was due to an increase in the real area of contact because of the wear evolution.

Energy Dissipated per cycle. Finally, in Fig. 3.4c the evolution of the energy dissipated per cycle is shown. Tests 4 and 5 have a higher energy dissipated per cycle than tests 1 and 2 since they featured a larger sliding displacement and, consequently, their hysteresis loops encompassed a larger area. The energy dissipated/cycle maintained a fairly constant value for the duration of all tests.

3.3.2. Evolution of Surfaces

Every wear test was performed using new test specimens polished and cleaned to the standard polishing and cleaning specification mentioned previously. After each fretting test, the contact interfaces were surrounded by red debris resulting from the oxidation of the fretted metal (e.g., see Fig. 3.1). This debris was removed by cleaning the specimens in an ultrasonic bath. The clean interfaces were then scanned with the optical interferometer. Fig. 3.1 shows the typical images, obtained from the interferometer, of one specimen before and after a wear test. A summary of the worn interfaces from all wear tests is provided in Fig. 3.5, where material transfer spots between coupled specimens are highlighted. The highlighted areas provide a

clear indication of material transfer between top and bottom specimens, suggesting that the dominant wear mechanism is adhesive. The material transfer took place at both smaller and larger sliding distances and also over short and long duration wear tests. The location and number of transfer areas appear random at a first glance and do not show a clear pattern. However, tests 1 and 2 (shorter sliding distance) present smaller and distributed transfer areas, while tests 3, 4 and 5 (larger sliding distance) present larger transfer areas. This is probably attributable to the fact that for a larger sliding distance the small wear scars merge into larger ones, since the transferred material can be pushed further.

In addition to that, some of the worn profiles show the typical "W-shaped" wear scar (see e.g. wear tests 3 and 5 in Fig. 3.5), which has been observed in many other studies [30, 46–50, 79–81], although only one of them involved a flat-on-flat contact arrangement [30]. This W-shape is a typical wear pattern consisting of a stick region, inside the fretted interface, surrounded by slip regions on both sides [50]. Fouvry et. al [81] investigated in detail the physics of the W-shape wear scars as opposed to the U-shape scars. They found that at lower contact pressures, a homogenized U-shaped wear scar generates as a result of abrasive wear in combination with high contact oxygenation. This oxygenation produces a thin oxide debris layer, which induces high energy wear rates and wear volumes. Instead, at higher contact pressures, W-shaped wear scars occur. The W-shaped scars are the result of (i) adhesive wear in the center of the scar, where the contact is stuck due to the higher pressure, and (ii) abrasive wear at the edges, where the pressure is lower and debris is generated due to the more severe wear induced by the increased slipping. In the present study, this kind of W-shaped wear scar is more evident in the second set of tests (3, 4 and 5) conducted for a larger sliding distance. This suggests that for larger sliding distances the adhesive wear in the central region may be activated, while at the edges of the contact abrasive wear is dominant. However, it is important to note that these phenomena are pressure dependent. In the study of Fouvry et al. [81] the contact was cylindrical-on-plane, resulting in larger pressures generally located in the center, while in present study a flat-on-flat contact was analyzed. In this case, the pressure distribution is more uncertain and depends on the waviness and overall shape of the interfaces.

The wear volume was also calculated by superimposing the optical interferometer images before and after wear tests, and then taking the difference in 3D topography. The result of this calculation is illustrated in Fig. 3.6, where the relationship is shown between the wear volume and the energy dissipated at the contact for different excitation amplitudes. The relationship is almost linear for the tests conducted at $22\mu m$ of sliding distance, confirming the previous findings from the literature [43–47, 71, 80–83]. The linear relationship is defined by a wear coefficient α that is the linear slope of wear volume versus cumulative energy dissipated as defined in [71]. In the case of tests at $22\mu m$ of sliding distance, this coefficient is roughly $\alpha \sim 1500\mu m^3/J$, and is of the same order of magnitude of the ones found in studies investigating ductile materials [71, 84] or one order of magnitude lower compared to other studies [45, 47, 80, 81, 85]. The two tests conducted at $14\mu m$ of sliding distance showed an almost similar wear volume, 4.3 and 5.2 $\mu m * mm^2$ respectively, since they dissipated almost the same amount of energy. The variability is below the 20% and this relatively small difference gives an idea of the measurements variability and could be due to the difficulty in measuring the wear volume accurately due to such small quantities and irregular worn area distributions. Additionally, the wear volume of tests 1 and 2 (conducted at $14\mu m$) is lower than the one obtained for the same energy dissipated but with a larger sliding distance (test 4 at $22\mu m$) and this would lead also to a lower wear coefficient. This is in accordance with the fretting maps concept proposed by Vingsbo and Söderberg [34], who observed that, in gross sliding, the wear coefficient increases with larger sliding distances. This means that, for the same cumulative energy dissipated, the wear volume is larger if also the sliding distance is larger. Fouvry et al. [44] described this behaviour by considering (i) the energy required to generate the debris (that contributes to the wear volume) and (ii) the energy successively required to expel such debris from the contact interface. The higher the sliding amplitude, the faster the debris is ejected and the lower is the energy required for expelling it. Therefore, for a larger sliding amplitude, less energy is required to expel the debris and, as a result, more energy is left to increase the wear volume. In other words, if the sliding amplitude is very small it is more likely that wear debris remains trapped under the surface and less new debris is generated. It should be pointed out that they investigated cylindrical contacts rather than flat-on-flat contacts.

On the contrary, in a more recent study, Pearson and Shipway [86] argued that the wear coefficient is not

9

Wear Test 1: 5.3 hrs

Top Specimen - Moving

Bottom Specimen - Stationary

$\Delta x = 14\ \mu m$

Sliding direction

200 µm

µm

9

0

-14

8

0

-16

Worn area = 1.17 mm^2

Worn area = 1.20 mm^2

Wear Test 2: 5.5 hrs

Top Specimen - Moving

Bottom Specimen - Stationary

$\Delta x = 14\ \mu m$

Sliding direction

200 µm

µm

12

0

-25

17

0

-27

Worn area = 1.03 mm^2

Worn area = 1.03 mm^2

Wear Test 3: 0.6 hrs

Top Specimen - Moving

Bottom Specimen - Stationary

$\Delta x = 22\ \mu m$

Sliding direction

200 µm

µm

11

0

-14

9

0

-24

Worn area = 0.82 mm^2

Worn area = 0.82 mm^2

Wear Test 4: 3.6 hrs

Top Specimen - Moving

Bottom Specimen - Stationary

$\Delta x = 22\ \mu m$

Sliding direction

200 µm

µm

20

0

-20

11

0

-19

Worn area = 1.17 mm^2

Worn area = 1.13 mm^2

Wear Test 5: 9 hrs

Top Specimen - Moving

Bottom Specimen - Stationary

$\Delta x = 22\ \mu m$

Sliding direction

200 µm

µm

15

0

-30

22

0

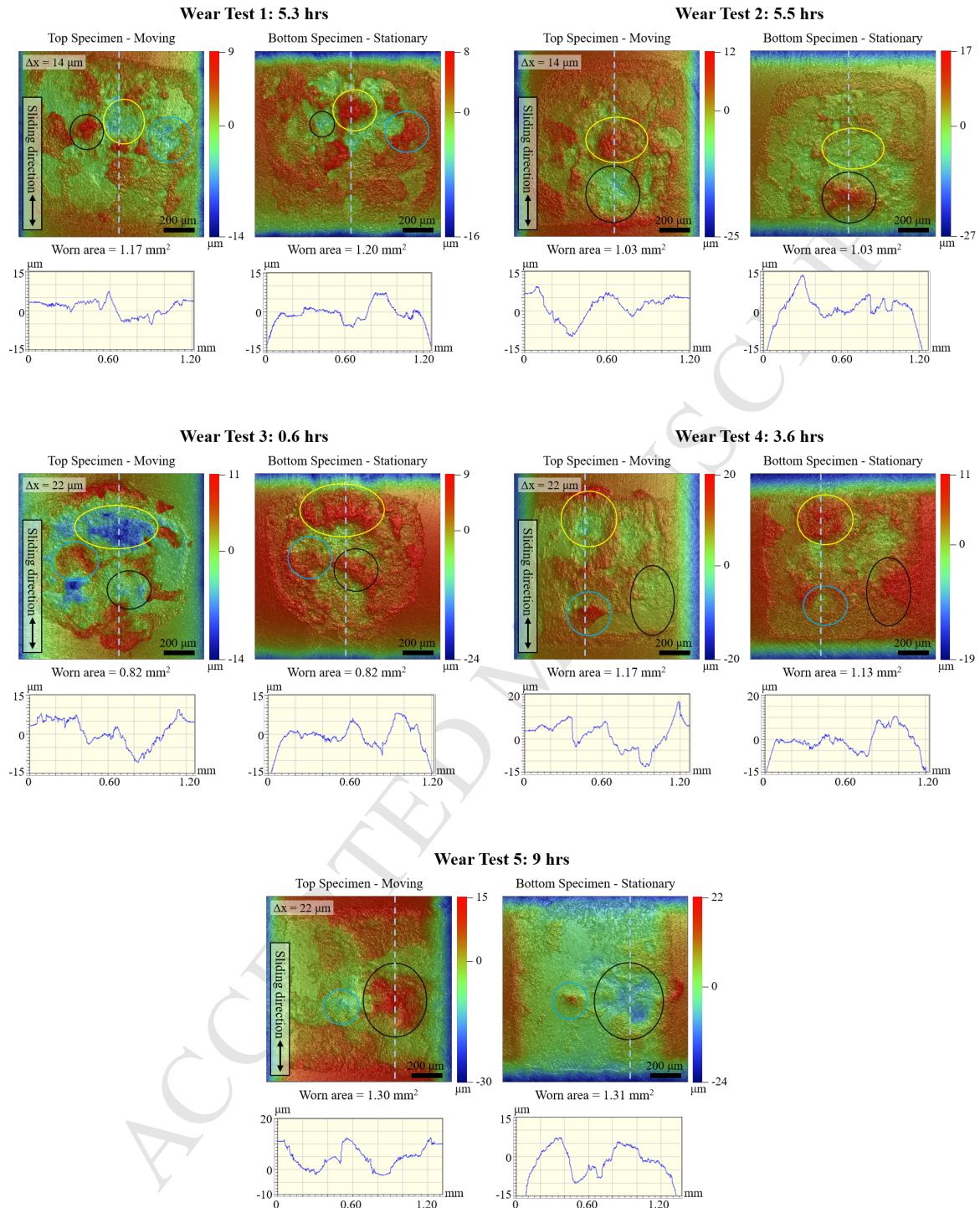-24

Worn area = 1.30 mm^2

Worn area = 1.31 mm^2

Figure 3.5: Worn surface images highlighting the material transfer between the top and bottom specimens for different test couples. The contact interfaces of the bottom specimens were opened and flipped to help the overlap comparison.

dependent on the sliding amplitude. It is expected that for the same cumulative energy dissipated, the wear coefficient, and hence the wear volume, are equal regardless of the sliding distance. The current results seem

10

to match better the first hypothesis, but future experiments will hopefully clarify this dependency of the wear coefficient on the sliding distance.
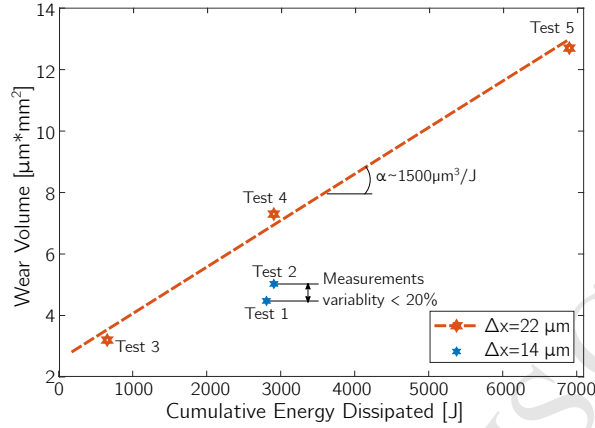

Figure 3.6: Wear volume as a function of energy dissipated at the contact. Test conditions: excitation frequency=100Hz, normal load=60N, nominal area of contact=$1mm^2$, material=Stainless Steel, temperature=25°C.

3.3.3. Evolution of the system dynamics

Before and after every wear test, a hammer test was conducted in order to obtain the frequency response functions (FRFs) of the friction rig. The hammer hit was made at the excitation point in place of the shaker attachment. An accelerometer was placed on the moving arm to measure the friction rig response. In Fig. 3.7 the test setup is shown together with the typical arm response. Three resonant frequencies are observed over the frequency range measured. The first natural frequency at 40Hz and the third at 2500Hz both refer to the horizontal motion mode, where the moving arm and moving mass move respectively in-phase and out-of-phase in the direction of sliding. These are the modes of interest since they are in the sliding direction and they are used to create a two degree of freedom model of the rig, which is described in Section 4. The second natural frequency at 700Hz is not a mode of interest, since it is a lateral rotation of the moving arm that does not affect the sliding of the specimens and, in addition, is far from the fretting test excitation frequency (100Hz).

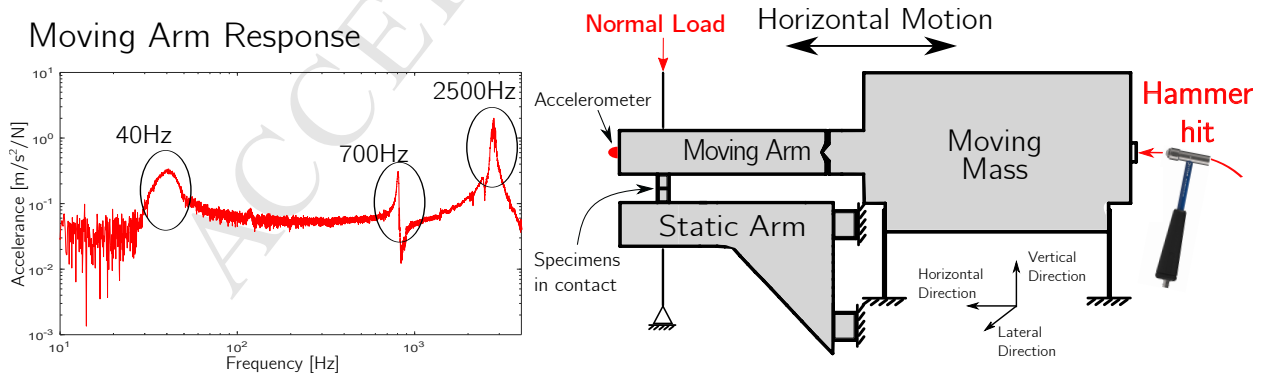It is expected that the horizontal modes are affected by the wear evolution of the specimens' contact

Figure 3.7: Hammer test setup. Modes: 40Hz is the horizontal motion of moving arm and moving mass in-phase; 700Hz is a lateral rotation of the moving arm; 2500Hz is the horizontal motion of moving arm and moving mass out-of-phase.

interfaces. To investigate this evolution, a hammer test was conducted before and after every wear test. Fig.

11

3.8 shows the FRFs obtained at 7N and 60N of normal load, in both cases before and after the wear test number 1 (the behaviour is the same for every other wear test). The 7N normal load was also investigated with hammer tests because when the pneumatic actuator was unloaded at the end of the test (or loaded at the beginning), a 7N normal load resulted in the contact due to the self-weight of the moving arm that lay on the static arm. Therefore, an additional hammer test was conducted in this 7N normal load condition, since it did not affect the wear test itself and could provide insights on the effect of different normal loads. Several conclusions are drawn from the FRFs:
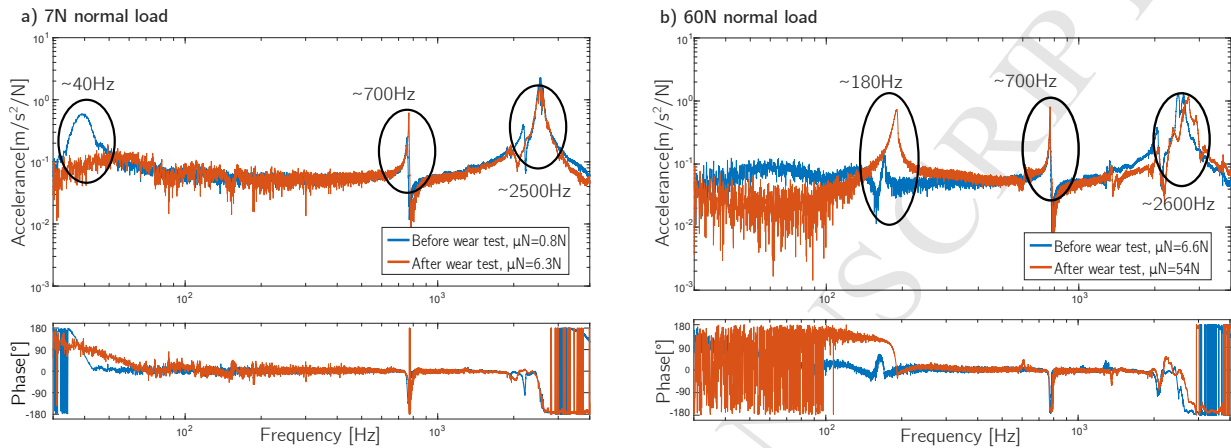

Figure 3.8: Evolution of system dynamics for test 1: a) 7N normal load; b) 60N normal load.

1) Effect of the normal load. The normal load strongly affects the first natural frequency. If the normal load is increased, also the natural frequency increases (from ~ 40Hz for 7N normal load to ~ 180Hz for 60N normal load). This happens because the two specimens enhance their conformity and the rig becomes stiffer. As the limit μN increases linearly with the normal load N, this reduces the amount of slipping (i.e. hysteresis loops are shorter, and the sticking regime becomes dominant). This reduction of slipping results in an stiffer system.

2) Effect of wear on modes in the sliding direction. The wear also strongly affects the first natural frequency. This is attributable to the evolution of both friction coefficient and contact stiffness (as already shown in Fig. 3.4). In fact, the increase in the friction coefficient leads to an increase in the friction limit, thus reducing the total amount of slip. This reduction in the amount of slip results in a stiffening of the contact, which is more likely to be in the stuck condition (the same effect occurred for an increased normal load, as shown in the previous paragraph). In addition, also the contact stiffness increases, thus making the system even stiffer. These two phenomena explain the shift to the right of the first natural frequency before and after the wear test.

Not only is the natural frequency of the system increases with wear, but also the damping changes. For the 7N normal load case, the damping increased with wear (i.e. lower and wider peak after wear). This happened because of the increase in the friction coefficient that led to hysteresis loops having larger friction limit and, therefore, having a larger area and energy dissipated. The more the energy dissipated, the more the peak is damped. However, in the case of 60N normal load, the peak reaches a higher value, indicating a reduction in damping. This is probably due to the fact that at 60N normal load the tendency to slip is reduced. Since after wear the friction limit increased, this tendency to slip is reduced even more (i.e. the system go towards a more stuck condition), thus reducing the total amount of energy dissipated.

3) Effect of wear on modes not in the sliding direction. The wear does not seem to affect modes that are not linked to the interface sliding. For example, the second mode (i.e. lateral rotation of the moving arm at 700Hz) is not affected by wear as shown in Fig. 3.8. The reason for this is not entirely clear, but probably this mode is characterized by a small relative sliding motion between the specimens.

Finally, during the test number 5 (the 9 hours test), the rig was stopped every 2.5 hours for allowing the shaker to cool. When the rig was stopped, hammer tests were conducted in order to further investigate the evolution of the rig dynamics. The tests were conducted without changing the normal load, which was maintained fixed at 60N. During these tests, time histories of the moving arm response were recorded. The goal was to extract the vibration amplitude dependency of both natural frequency and damping ratio related to the first horizontal mode. To extract information on this mode of interest, a Butterworth filter was used [87]. Filtering data is a standard practice in multi-modal analysis and is valid as long as there is good separation between the modes of interest so that a multi-modal system can be treated as a single degree of freedom system at each mode. The Butterworth filter was applied to the raw signal of the acceleration, and in this way the information related to the frequency range of the only first mode was isolated, see Fig. 3.9a. Subsequently, a Hilbert transform [88–90] was performed on the filtered signal. The Hilbert transform is a linear operator that generates the envelope of the amplitude of a decaying time history as shown in Fig. 3.9b. This envelope is then used to obtain the natural frequency and damping ratio as functions of the vibration amplitude, see Fig. 3.9c-d. The Hilbert transform was chosen due to its high accuracy in extracting these parameters from ring down data [91]. Other methods, such as wavelet-based approaches, are more suitable for studying modal interactions within dynamic systems [92]. As expected, both natural frequency and damping are not constant and strongly vary as the amplitude of the vibration decays. The natural frequency increases with wear, due to the increase in both friction coefficient and contact stiffness, and it seems to be not much affected by the acceleration amplitude (and therefore the by sliding distance) of the moving arm. Instead, the damping increases with the amplitude. This is not surprising since at larger accelerations (and therefore larger sliding) hysteresis loops become wider, resulting in higher energy dissipated and therefore higher damping. Moreover, the damping ratio reduces as the test goes on, meaning that the system dissipate less energy as wear increases. This trend is in accordance with Fig. 3.8b, since after wear the peak is less damped because the increases in both friction coefficient and contact stiffness reduce the tendency of the system to slip.
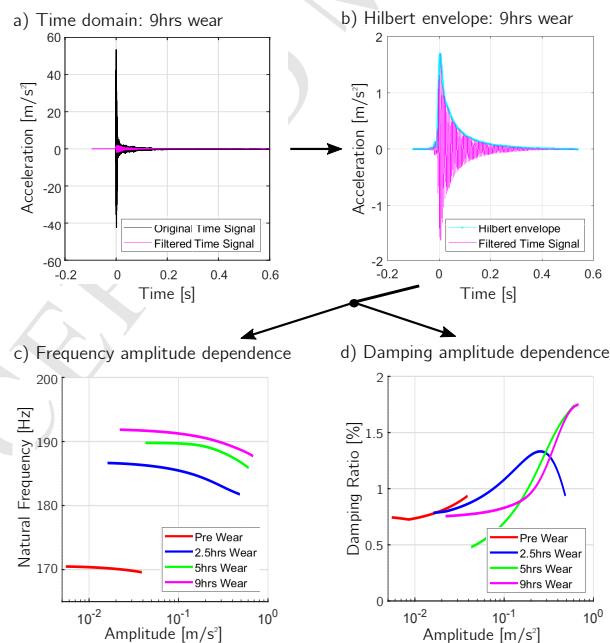

Figure 3.9: Hilbert analysis to capture the evolution of the first natural frequency during test 5: a) Time signal at the end of the test; b) Hilbert envelope of the filtered signal; c-d) Amplitude dependencies of natural frequency and damping ratio obtained from the Hilbert envelopes.

3.4. Experimental Analysis Discussion

Experiments were conducted using a friction rig for hysteresis measurements. Wear tests were performed under high frequency excitations over different time spans to better understand their impact on the system dynamics (wear tests' specifications are summarized in Table 3.1). The obtained data has shown that wear affects the evolution of contact parameters in the case of the analysed stainless steel specimens. Both friction coefficient and contact stiffness increase with fretting cycles before they reach a steady state.

The main novelty of this work is the study of the effects of wear on the dynamic response of a system with a frictional joint (i.e. the friction rig). The obtained results show that wear can strongly affect the dynamic behaviour of the system, leading to shifts in natural frequencies and damping, and has a particular influence on the modes that activate the contact mechanisms (i.e. the modes in the same direction of the fretting sliding).

The first effect of wear is the increase in the natural frequency of such modes over time (see Fig. 3.8). This change in the natural frequency with wear is due to the increase in both friction coefficient and tangential contact stiffness. These increases lead to a higher conformity of the contact interfaces that are more inclined in being stuck rather than slipping. This increased sticking results in an overall stiffening of the system in a combination with a consequent increase of the natural frequencies of the modes linked to the contact mechanisms. For the investigated structure, the main factor affecting the dynamics is in fact the friction limit, μN, at which the contact start to slide. The friction limit depends on the value of the friction coefficient, which is strongly affected by wear.

Damping is also affected by wear, and results show that it can either increase or decrease depending on whether the system raises or lowers the amount of energy dissipated within each hysteresis loop. If the system before wear is already close to a fully stuck condition (e.g. the normal load is high, and the macroslip regime is minimal), then, after wear, the observed increase in the friction coefficient further reduces the tendency of the system to slip, thus resulting in a damping reduction due to the reduced dissipated energy (see Fig. 3.8b: μN before wear is 6.6N and after wear is 54N). In contrast, at low normal loads, it is more likely that the system is in full slip and the increase in the friction coefficient over time would result in hysteresis loops having a larger area due to the increase in the friction limit. The larger area results in more energy dissipated at the contact, which in turn increases the damping of the system over time (see Fig. 3.8a: μN before wear is 0.8N and after wear is 6.3N).

It is also interesting to note that the FRF measured for the 7N normal load case after wear is quite similar to the FRF measured at 60N normal load before wear. This is due to the fact that in both cases the friction limit is similar too. At 7N normal load, the after wear friction coefficient is 0.9, leading to a friction limit $\mu N = 6.3N$. At 60N normal load, the before wear friction coefficient is 0.11, leading to a friction limit $\mu N = 6.6N$. The two similar friction limits lead to a similar dynamic behaviour, confirming the significant effect of the amount of sliding on the dynamics of the system.

For completeness it should be noted that modes that do not activate the interface mechanisms are unaffected by the interfacial wear and are therefore independent of time.

Finally, the Hilbert analysis of the time history data has shown that the damping is displacement-dependent. This is not surprising since larger displacements generate wider hysteresis loops, which result in more energy dissipated at the contact.

Due to the large impact that wear has on the dynamic response and to the complexity of the mechanisms at play at the interface, a numerical analysis approach was introduced in order to capture the evolution of the hysteresis loops and the dynamic behaviour of the rig over time.

4. Numerical Analysis

In order for the results of this experimental study to be accessible for modeling and design in structural dynamics, a physically-based, wear evolving Bouc-Wen model is proposed (based on the work of [93] and [94]), and a numerical analysis is performed on a two degree of freedom lumped mass model of the test rig.

4.1. Lumped mass model of the test rig

A simplified lumped mass model of the test rig was created in order to simulate the rig dynamics. As already shown in Section 3.3.3, two resonant modes are of interest: the in-phase and out-of phase horizontal modes. In order to represent them, a two degree of freedom (2DOF) lumped model was carefully created based on an hammer test campaign that, for simplicity, is not presented here. The model is shown in Fig. 3.2c and the values of the system parameters are presented in Table 4.1. m_1 and m_2 are the moving mass and moving arm respectively. The moving mass is connected to the ground by means of leaf springs having stiffness k_1 (see Fig. 3.2b). The moving arm is hinged to the moving mass by means of a knife edge having stiffness k_2. The moving arm is connected to the static arm (that is considered completely rigid) by means of a Bouc-Wen element, which is one of the many contact models used in dynamic simulations for the replication of hysteresis loops. The excitation F_{ex} is applied on the moving mass and the normal load N is applied on the moving arm (to maintain the specimens in a continuous contact). The Bouc-Wen element generates a friction force as a result of the relative displacement of the moving arm with the ground (i.e. with the static arm). The plot of this frictional force versus the relative displacement is the hysteresis loop. The first natural frequency of this model oscillates between 40 and 180Hz depending on the normal load, and the frequency values coincide with the experimental measured ones (the effects of the normal load on the natural frequency were already presented in Section 3.3.3). Also the natural frequency of the out-of-phase horizontal mode coincides with the experimental one, which oscillates between 2500 and 2600Hz.

In order to obtain the numerical forced response (i.e. the FRFs) of the test rig, the following set of equations of motion has to be solved:

$$\mathbf{M}\ddot{\mathbf{x}}(t) + \mathbf{C}\dot{\mathbf{x}}(t) + \mathbf{K}\mathbf{x}(t) = \mathbf{F_{ex}}(t) + \mathbf{F_f}(\mathbf{x}, \dot{\mathbf{x}}) \tag{1}$$

where M, C and K are respectively the mass, damping and stiffness matrices of the lumped model. $\ddot{x}, \dot{x}, x$ are the acceleration, velocity and displacement of the degrees of freedom of the lumped model, F_{ex} is the input excitation force and $F_f(\mathbf{x}, \dot{\mathbf{x}})$ is the friction force.

The input of the equations of motion are the mass, damping and stiffness matrices of the model and the excitation force, which is either coming from the hammer test or from the shaker test. The unknowns are the displacements (and velocities and accelerations) and the friction force. The friction force is predicted by the Bouc-Wen model, which is described in the next paragraph. Eq. 1 is solved using a Newmark time integration scheme [18]. Once the equation is solved, it is possible to plot the FRF of the moving arm (that is simply the acceleration of the arm (m_2) divided by the excitation force over the investigated frequency range). This FRF will be compared to the experimental ones. Additionally, also the hysteresis loops are obtained, since they are given by the friction force plotted versus the displacement of the moving arm.

Table 4.1: System parameters of the 2DOF model of the test rig.

Moving mass	m_1	21.2 kg
Moving arm	m_2	1.2 kg
Leaf spring stiffness	k_1	1.4 $N/\mu m$
Knife edge stiffness	k_2	273 $N/\mu m$

4.2. Description of the Bouc-Wen model

Several contact models are used in dynamics simulations for replicating hysteresis loops [95]. These models are classified into macroslip models (such as the well known Jenkins element [5, 6]) and microslip models (such as Iwan [1, 2], Valanis [7], LuGre [8] and Bouc-Wen [9, 10]). In this paper a Bouc-Wen formulation has been chosen to replicate hysteresis loops since its input parameters were physically linked to the experimental parameters.

The original Bouc-Wen formulation allows to recreate generic hysteresis loops [9, 10], not necessarily linked to frictional hysteresis. The model takes as input a relative displacement, and generates as output an

hysteretic force. By plotting this force versus the relative displacement, an hysteresis loop is generated. In this paper, the hysteretic force is the friction force F_f of Eq. 1, and it can be expressed as function of a variable z. The new variable z is the Bouc-Wen hysteresis variable which is governed by its own time dependant differential equation:

$$\mathbf{F_f}(\mathbf{x}, \dot{\mathbf{x}}) = \mathbf{z}(\mathbf{z}, \mathbf{x}, \dot{\mathbf{x}}) \tag{2}$$

$$\dot{z} = A\dot{x} - \beta |\dot{x}| |z|^{n-1} z - \gamma \dot{x} |z|^n \tag{3}$$

This differential equation allows for the replication of hysteresis loops and it depends on the displacement x, on the z itself and on 4 parameters that govern the shape of the resulting hysteresis loop: A, β, γ and n. The influence of these parameters has been widely studied, as reviewed for example by Ismail et al. [96], but they pointed out that finding a physical interpretation for each of these parameters was not possible as each of them (i) could strongly affect the global aspect of the hysteresis loop shape and (ii) is sensitive to the variations of the others. A more physical Bouc-Wen formulation is therefore needed to describe friction phenomena. This formulation has been obtained by normalizing the original equation, as already performed by Guo et al. [93], who proposed a normalized Bouc-Wen model for the modelling of frictional hysteresis. In short, they introduced new normalized parameters defined as follows:

$$z_0 = \left(\frac{A}{\beta+\gamma}\right)^{\frac{1}{n}}, \qquad \rho = \frac{A}{z_0} > 0,$$
$$\sigma = \frac{\beta}{\beta+\gamma} \geq 0, \qquad \xi = \frac{z}{z_0} \in [-1; 1]$$

This formulation leads to a normalized Bouc-Wen variable ξ which varies in $[-1; 1]$. This variable ξ is simply a normalized hysteresis loop that varies between the force limits -1 and 1 (when there is full sliding). The general Bouc-Wen model expressed in Eq. 3 can be rewritten as:

$$\begin{cases} z = z_0 \xi \\ \dot{\xi} = \rho(1 - (\sigma \operatorname{sgn}(\dot{x}) \operatorname{sgn}(\xi) + 1 - \sigma) |\xi|^n)\dot{x} \end{cases} \tag{4}$$

which is equivalent to its original form. Furthermore, the friction component from Eq. 2 can be rewritten as:

$$\mathbf{F_f}(\mathbf{x}, \dot{\mathbf{x}}) = z_0 \boldsymbol{\xi}(\boldsymbol{\xi}, \boldsymbol{x}, \dot{\boldsymbol{x}}) \tag{5}$$

The advantage of writing the Bouc-Wen model as in Eq. 4 is that the parameters can now be physically linked. In fact, z_0 defines the friction limit μN, where μ is the friction coefficient and N is the normal load applied to the system. ρ plays the role of the contact stiffness and is equal to $\frac{k_t}{\mu N}$, where k_t is the experimental contact stiffness. $n \geq 1$ controls the microslip region and σ, the global shape of the hysteresis loop. This formulation facilitates modeling as the physical parameters are more intuitive than the non-physical parameters used in a traditional formulation.

One problem that arises using this model, is that during the macroslip regime the friction limit becomes completely flat (since $\xi = 1$ or -1), while experimentally, a slope in the macroslip region may appear (see the macroslip slope in Fig. 4.1). To counter this problem, an additional term, $k_p \Delta x$ is added to the friction model from Eq. 5, which can be seen as an additional linear stiffness in the problem. The friction model becomes:

$$\mathbf{F_f}(\mathbf{x}, \dot{\mathbf{x}}) = k_p \boldsymbol{\Delta x} + \mu N \boldsymbol{\xi}(\boldsymbol{\xi}, \boldsymbol{x}, \dot{\boldsymbol{x}}) \tag{6}$$

However, this additional stiffness leads to a change of contact stiffness in the hysteresis loop. To remove it, the stiffness parameter present in the Bouc-Wen equation (ρ) shall be now modified as $\rho = \frac{k_t - k_p}{\mu N}$.

A typical hysteresis loop obtained using this modified Bouc-Wen formulation is shown in Fig. 4.1, and it is compared to the experimental one. The exact values of μN, k_t and k_p were extracted from the experimental curves and injected into the Bouc-Wen model. The experimental loops are very well replicated.
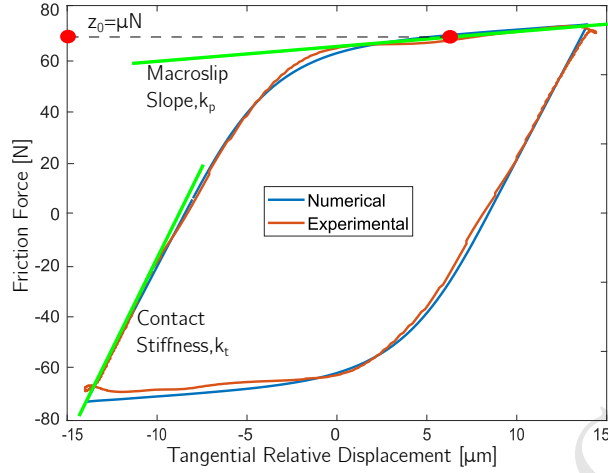
16

Figure 4.1: Comparison between an experimental and numerical hysteresis loop using as input the exact experimental parameters.

4.2.1. Introduction of the wear evolution in the Bouc-Wen friction model

One shortcoming of the existing physically based Bouc-Wen models is that they do not include wear evolution. To account for this, the results of [94], which modified the original Bouc-Wen formulation to account for degradation of the hysteresis loops, is introduced here. The principle of the form proposed in [94] is that a function is defined to represent the degradation of the other parameters in the model. Here, this idea is introduced to the physically based model of Eq. 4 by defining a set of wear functions that describe how the physical parameters evolve. These evolving parameters are the contact stiffness k_t, the macroslip slope k_p and the friction coefficient μ, and they are all pre-multiplied by their respective wear functions. The wear functions, called f_μ, f_{k_p} and f_{k_t}, can take any form which is in agreement with experimental curves, as the ones shown in Fig. 3.4a-b, and they can be formulated as a function of time but also of the dissipated energy. In this case, the functions were made energy dependent.

The modified Bouc-Wen model that takes the evolution of wear into account takes the form of:

$$\begin{cases} \mathbf{F_f}(\mathbf{x}, \dot{\mathbf{x}}) = f_{k_p}(E)k_p \boldsymbol{\Delta x} + f_\mu(E)\mu N \boldsymbol{\xi}(\boldsymbol{\xi}, \boldsymbol{x}, \dot{\boldsymbol{x}}) \\ \dot{\xi} = \frac{f_{k_t}(E)k_t - f_{k_p}(E)k_p}{f_\mu(E)\mu N}(1 - (\sigma\, \mathrm{sgn}\,(\dot{x}\xi) + 1 - \sigma)\,|\xi|^n)\dot{x} \end{cases} \tag{7}$$

where a typical wear function can be of the form:

$$f(E) = 1 + a\, e^{-\frac{b}{E}} \tag{8}$$

Here, a and b depend respectively on the maximum amplitude and the quickness at which the steady state is reached. When $E = 0$, then $f(E) = 1$ and therefore the initial value of the parameter is obtained, since it becomes just pre-multiplied by 1. When $E \to \infty$, $f(E) = a + 1$, which leads to the steady state observed experimentally and a is therefore the normalized change of amplitude of the contact parameter. This newly modified Bouc-Wen formulation has been used to obtain the numerical results. Please note that the wear functions can be applied to any contact model whose evolution of the contact parameters with wear is known. In fact, this formulation is also valid for Jenkins elements [5, 6] or a Valanis model [7] for example.

4.3. Numerical Results

To simulate the evolution of wear with respect to the energy dissipated, a Newmark time integration scheme was used to solve Eq. 1, where the friction force F_f was calculated by solving Eq. 7 from the modified Bouc-Wen model. At each time step, the energy dissipated was computed and the contact parameters (ρ, μ

17

and k_p) were updated.

Fig. 4.2a shows the evolution of the numerical hysteresis loops with respect to the increase of the dissipated energy. The trend is similar to what was observed experimentally. In fact, the slope of the stick portion of the loops (i.e. the contact stiffness) increases together with the dissipated energy, as well as the macroslip slope and the friction force. This confirms the validity of the proposed method to simulate the evolution of wear in frictional contacts. Several of these curves were superimposed with the experimental ones for the test 1, as shown in Fig. 4.2b. The match is in a very good agreement.

The evolution of the friction coefficient μ and the contact stiffness k_t are illustrated in Fig. 4.2c and 4.2d respectively, and compared with the experimental results for the wear test 1, showing again a very good agreement with experiments. This suggests that the wear functions used for the fitting are adequate. Table 4.2 shows a summary of the Bouc-Wen parameters used to generate Fig. 4.2.

Table 4.2: Bouc-Wen parameters used to replicate test 1.

	Value	Wear Function	Parameters
μ	0.11	$f_\mu(E) = 1 + b \cdot log(aE + 1)$	a=1.3e9; b=0.26
k_t	27.3	$f_{k_t}(E) = 1 + a\ e^{-\frac{b}{E}}$	a=1.32; b=150
k_p	0.88	$f_{k_p}(E) = 1 + aE$	a=0.24
σ	0.5	/	/
n	2	/	/

Finally, the FRFs of the system were predicted for the cases before and after wear, at 7N and 60N of normal load, in order to address a comparison with the experimental ones shown in Fig. 3.8. The input excitation force used for the numerical simulation is exactly the same of the hammer test. The FRF was obtained by plotting the acceleration (from the solution of Eq. 1) over the input force, for the range of frequency of interest. In Fig. 4.3 the numerical FRFs are shown. The results are quite promising since they follow the same trend of the experimental FRFs shown in Fig. 3.8. For both normal loading conditions, the natural frequency of the first peak increases after wear. In addition, for the 7N normal load case the peak is more damped, while for the 60N normal load case the peak is less damped.

There is a very good agreement between the trends shown in the experimental FRFs (Fig. 3.8) and the numerical predictions (Fig. 4.3). This is a promising result as the only calibration performed was to match the experimental evolution of friction coefficient and contact stiffness with the numerical evolution by means of the wear functions (Fig. 4.2c-d and Table 4.2). The evolution of these contact parameters corresponded to a wear experiment conducted at 60N normal load. Nevertheless, the model performed well even outside of the calibrated regime of 60N, predicting the correct trend of the FRFs also for the 7N normal load case. The striking result is that the simple 2DOF model is able to replicate the dynamic behaviour of the system even outside of the calibrated regime. It confirms that the system becomes stiffer with wear (i.e. the natural frequency increases) due to the increases in friction coefficient, friction limit and contact stiffness. Damping is also well replicated, confirming the reliability of the numerical approach, but also highlighting the good quality of the experimental measurements that feed the friction model.

The newly proposed wear formulation has shown a very good capability in representing the evolution of both hysteresis loops and system's dynamics. The proposed wear functions are not restricted to the Bouc-Wen model. Indeed, they can be easily applied to every contact model that takes as input physical parameters that evolve with wear such as contact stiffnesses and friction coefficient.
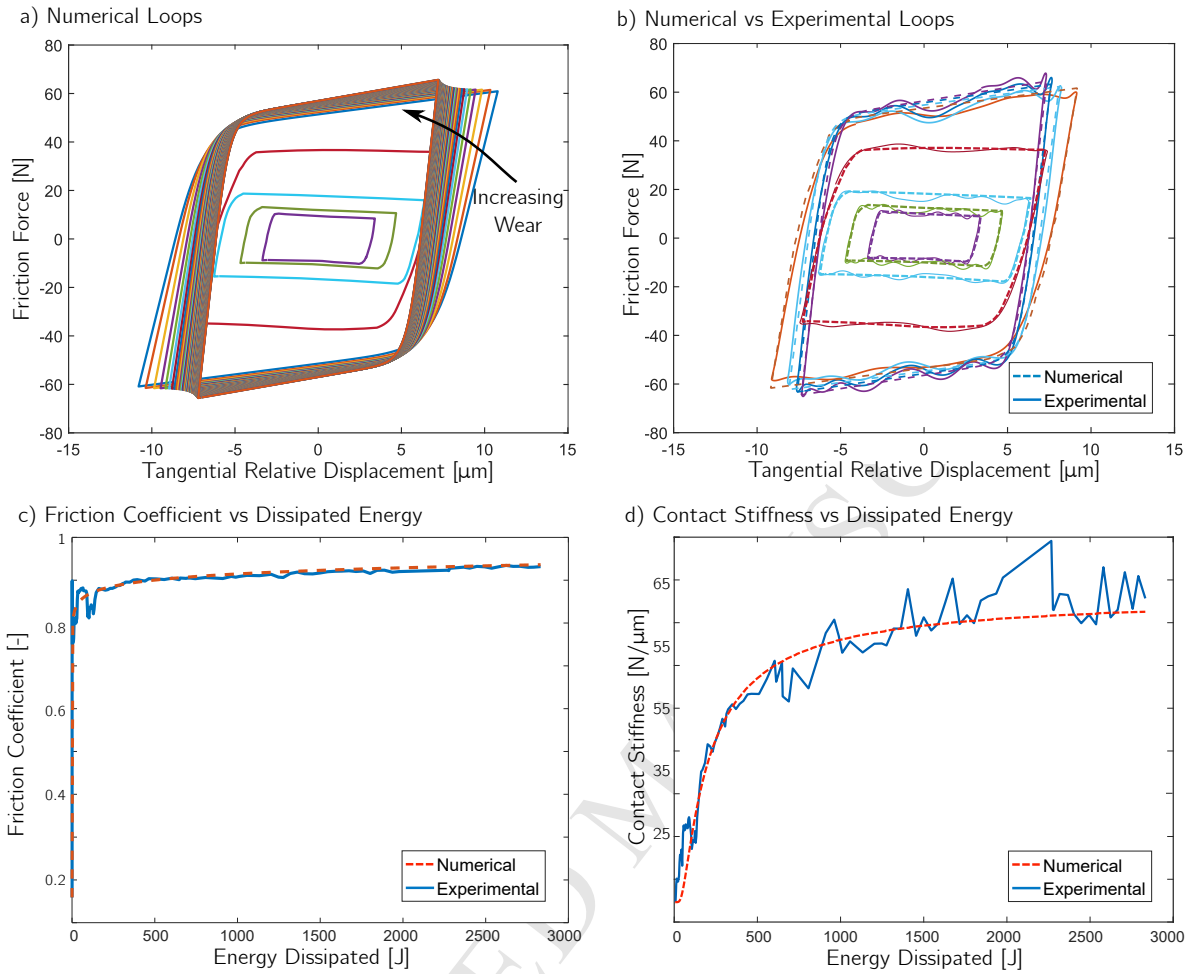
Figure 4.2: Comparison between numerical and experimental results: a) numerical loops; b) numerical loops vs experimental loops for test 1; c) friction coefficient vs energy dissipated for test 1 (wear function defined in Table 4.2); d) contact stiffness vs energy dissipated for test 1 (wear function defined in Table 4.2).
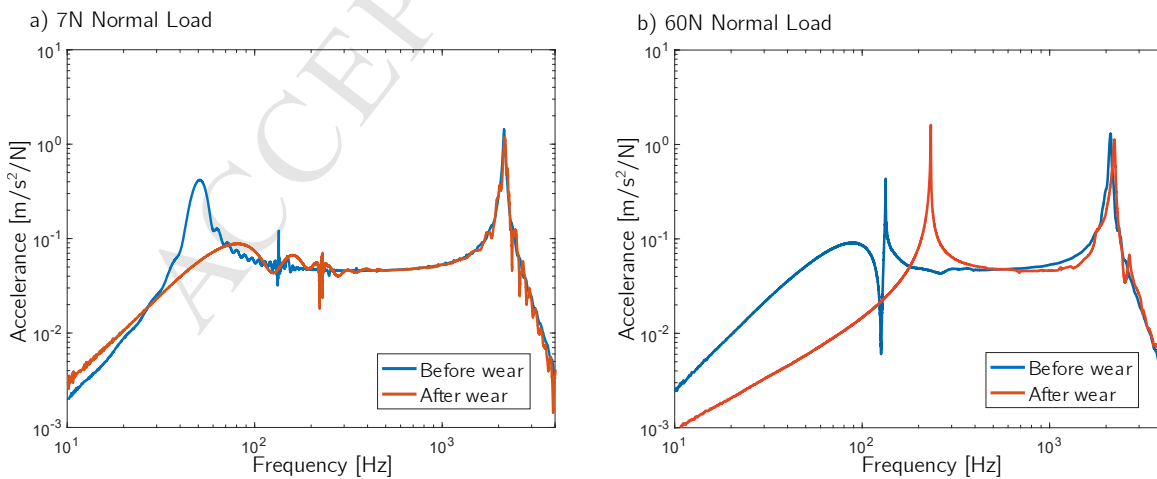

Figure 4.3: Numerical FRFs, before and after wear, based on the input hammer excitation of the test 1: a) 7N normal load; b) 60N normal load. Compare with the experimental FRFs in Fig. 3.8.

5. Conclusions

This paper presented a combined experimental and numerical investigation of the effects of wear on the evolution of both frictional contacts and system dynamics. This was accomplished by conducting a series of fretting wear tests using a friction rig for hysteresis measurements. Hysteresis loops and rig dynamics were recorded to assess the effect of wear. Additionally, a numerical analysis was performed to replicate experimental measurements. A time integration scheme was used to solve the equations of motion and a newly, wear evolving, physically based Bouc-Wen model of frictional hysteresis has been proposed.

The major conclusions and outcomes of this work are:

- To the authors' knowledge, this is the first time that the impact of wear on the dynamics of a structure has been experimentally quantified.

- Wear leads to significant shifts in natural frequency and damping of vibration modes of the structure, due to changes in friction coefficient, tangential contact stiffness and normal load. However, vibration modes that do not activate contact mechanisms (i.e. they are not in the sliding direction) seem not to be affected by the wear evolution of the interfaces.

- Both friction coefficient and tangential contact stiffness increased within the first fretting cycles before reaching a steady state. One hypothesis for this behaviour that is currently being tested is that the rapid change in the coefficient of friction during the running-in regime is dominated by the removal of initial surface oxide layers, and the longer-term change in contact stiffness is due to the evolution in conformity of the contact interfaces.

- A novel and simple formulation has been proposed to account for wear in contact models used for dynamic simulations. The formulation is based on wear functions that pre-multiply the contact parameters that are most affected by the fretting wear.

- Wear needs to be included in models to correctly capture the dynamics of jointed structures over the lifetime of system.

The contribution of this paper is of particular relevance to the structural dynamics research community. These contributions pave the way for a better and more accurate modelling of the dynamics of jointed structures, with the aim of creating predictive models for an optimal design of components and for the prediction of catastrophic failures.

6. Acknowledgments

References

[1] W. D. Iwan, A Distributed-Element Model for Hysteresis and Its Steady-State Dynamic Response, Journal of Applied Mechanics 33 (4) (1966) 893–900. doi:10.1115/1.3625199.
URL http://appliedmechanics.asmedigitalcollection.asme.org/article.aspx?articleid=1397974

[2] D. J. Segalman, A Four-Parameter Iwan Model for Lap-Type Joints, Journal of Applied Mechanics 72 (5) (2005) 752–760. doi:10.1115/1.1989354.
URL http://appliedmechanics.asmedigitalcollection.asme.org/article.aspx?articleid=1415458{%}5Cnhttp://prod.sandia.gov/techlib/access-control.cgi/2002/023828.pdf

[3] C. Menq, J. Bielak, J. H. Griffin, The Influence of Microslip on Vibratory Response, Part I: a New Microslip Model, Tech. Rep. 2 (1986).

[4] B. D. Yang, C. H. Menq, Characterization of 3D Contact Kinematics and Prediction of Resonant Response of Structures Having 3D Frictional Constraint, Journal of Sound and Vibration 217 (5) (1998) 909–925.

[5] G. Jenkins, Analysis of the stress-strain relationships in reactor grade graphite, British Journal of Applied Physics 13 (1) (1962) 30–32. doi:10.1088/0508-3443/13/1/307.

[6] J. H. Griffin, Friction Damping of Resonant Stresses in Gas Turbine Engine Airfoils, Journal of Engineering for Power 102 (2) (1980) 329–333. doi:10.1115/1.3230256.
URL http://dx.doi.org/10.1115/1.3230256

[7] K. C. Valanis, Fundamental consequences of a new intrinsic time measure: Plasticity as a limit of the endochronic theory, Arch. Mech. Stos. 32 (1980) 171–191.

[8] C. Canudas de Wit, H. Olsson, K. Astrom, P. Lischinsky, A new model for control of systems with friction, IEEE Transactions on Automatic Control 40 (3) (1995) 419–425. doi:10.1109/9.376053.
URL http://ieeexplore.ieee.org/document/376053/

[9] R. Bouc, A Mathematical Model for Hysteresis, Acustica 24 (1) (1971) 16–25.

[10] Y.-K. Wen, Method for Random Vibration of Hysteretic Systems, Nanotechnology 8287 (1976) 142–145. doi:10.1002/mop.

[11] M. Brake, A reduced Iwan model that includes pinning for bolted joint mechanics, Nonlinear Dynamics 87 (2) (2017) 1335–1349. doi:10.1007/s11071-016-3117-2.

[12] E. P. Petrov, D. J. Ewins, State-of-the-art dynamic analysis for non-linear gas turbine structures, Proceedings of the Institution of Mechanical Engineers, Part G: Journal of Aerospace Engineering 218 (3) (2004) 199–211. doi:10.1243/0954410041872906.

[13] A. Cardona, T. Coune, A. Lerusse, M. Geradin, A multiharmonic method for non-linear vibration analysis, International journal for numerical methods in engineering 37 (9) (1994) 1593–1608.

[14] K. Sanliturk, D. Ewins, Modelling Two-Dimensional Friction Contact and Its Application Using Harmonic Balance Method, Journal of Sound and Vibration 193 (2) (1996) 511–523. doi:10.1006/jsvi.1996.0299.
URL http://www.sciencedirect.com/science/article/pii/S0022460X96902990

[15] S. Zucca, C. M. Firrone, Nonlinear dynamics of mechanical systems with friction contacts: Coupled static and dynamic Multi-Harmonic Balance Method and multiple solutions, Journal of Sound and Vibration 333 (3) (2014) 916–926. doi:10.1016/j.jsv.2013.09.032.

[16] C. Gastaldi, A. Fantetti, T. Berruti, Forced Response Prediction of Turbine Blades with Flexible Dampers: The Impact of Engineering Modelling Choices, Applied Sciences 8 (1). doi:10.3390/app8010034.
URL http://www.mdpi.com/2076-3417/8/1/34

[17] R. Lacayo, L. Pesaresi, J. Gross, D. Fochler, J. Armand, L. Salles, C. W. Schwingshackl, M. S. Allen, M. Brake, Nonlinear modeling of structures with bolted joints : a comparison of two approaches based on a time-domain and frequency-domain solver, Mechanical Systems and Signal Processing (114) (2019) 413–438.

[18] N. M. Newmark, A method of computation for structural dynamics, Journal of the engineering mechanics division 85 (3) (1959) 67–94.

[19] N. N. Balaji, M. R. Brake, The surrogate system hypothesis for joint mechanics, Mechanical Systems and Signal Processing 126 (2019) 42–64. doi:10.1016/j.ymssp.2019.02.013.

[20] C. W. Schwingshackl, D. Di Maio, I. Sever, J. S. Green, Modeling and Validation of the Nonlinear Dynamic Behavior of Bolted Flange Joints, Journal of Engineering for Gas Turbines and Power 135 (122504) (2013) 1–8. doi:10.1115/1.4025076.

[21] E. Cigeroglu, N. An, C.-H. Menq, Forced Response Prediction of Constrained and Unconstrained Structures Coupled Through Frictional Contacts, Journal of Engineering for Gas Turbines and Power 131 (022505) (2009) 1–11. doi:10.1115/1.2940356.

[22] E. P. Petrov, Method for Sensitivity Analysis of Resonance Forced Response of Bladed Disks With Nonlinear Contact Interfaces, Journal of Engineering for Gas Turbines and Power 126 (2009) 654–662. doi:10.1115/1.2969094.

[23] S. Zucca, C. M. Firrone, M. Gola, Modeling underplatform dampers for turbine blades: A refined approach in the frequency domain, JVC/Journal of Vibration and Control 19 (7) (2013) 1087–1102. doi:10.1177/1077546312440809.

[24] L. Pesaresi, L. Salles, A. Jones, J. S. Green, C. W. Schwingshackl, Modelling the nonlinear behaviour of an underplatform damper test rig for turbine applications, Mechanical Systems and Signal Processing 85 (2017) 662–679. doi:10.1016/j.ymssp.2016.09.007.

[25] A. Fantetti, C. Gastaldi, T. Berruti, Modelling and testing flexible friction dampers : challenges and peculiarities, Experimental Techniques 42 (4) (2018) 407–419.

[26] C. Siewert, L. Panning, A. Schmidt-fellner, A. Kayser, The estimation of the contact stiffness for directly and indirectly coupled turbine blading, in: Proceedings of ASME Turbo Expo 2006: Power for Land, Sea and Air, 2006.

[27] C. W. Schwingshackl, E. P. Petrov, D. J. Ewins, Effects of Contact Interface Parameters on Vibration of Turbine Bladed Disks With Underplatform Dampers, Journal of Engineering for Gas Turbines and Power 134 (3) (2012) 032507. doi:10.1115/1.4004721.
URL http://gasturbinespower.asmedigitalcollection.asme.org/article.aspx?articleid=1429804

[28] C. W. Schwingshackl, Measurement of friction contact parameters for nonlinear dynamic analysis, Topics in Modal Analysis

21

I 5 (2012) 167–177. doi:10.1007/978-1-4614-2425-3_16.

[29] M. Lavella, D. Botto, M. M. Gola, Design of a high-precision, flat-on-flat fretting test apparatus with high temperature capability, Wear 302 (1-2) (2013) 1073–1081. doi:10.1016/j.wear.2013.01.066.
URL http://dx.doi.org/10.1016/j.wear.2013.01.066

[30] M. E. Kartal, D. M. Mulvihill, D. Nowell, D. A. Hills, Measurements of pressure and area dependent tangential contact stiffness between rough surfaces using digital image correlation, Tribology International 44 (10) (2011) 1188–1198. doi:10.1016/j.triboint.2011.05.025.
URL http://dx.doi.org/10.1016/j.triboint.2011.05.025

[31] L. Pesaresi, J. Armand, C. W. Schwingshackl, L. Salles, C. Wong, An advanced underplatform damper modelling approach based on a microslip contact model, Journal of Sound and Vibration 436 (2018) 327–340. doi:10.1016/j.jsv.2018.08.014.

[32] R. B. Waterhouse, Fretting wear, Wear 100 (1984) 107–118. doi:10.1016/0043-1648(84)90008-5.

[33] R. B. Waterhouse, Fretting fatigue, International Materials Reviews 37 (1) (1992) 77–98. doi:10.1179/imr.1992.37.1.77.
URL https://doi.org/10.1179/imr.1992.37.1.77

[34] O. Vingsbo, S. Söderberg, On fretting maps, Wear 126 (1988) 131–147. arXiv:0810.4096, doi:10.1016/0043-1648(88)90134-2.

[35] J. Greenwood, J. Williamson, Contact of nominally flat surfaces, Proceedings of the Royal Society London A 1442 (295) (1966) 300–319.

[36] S. Medina, D. Nowell, D. Dini, Analytical and numerical models for tangential stiffness of rough elastic contacts, Tribology Letters 49 (1) (2013) 103–115. doi:10.1007/s11249-012-0049-y.

[37] H. Hertz, Uber die Beruhrung fester elasticher Korper, Jnl. reine und angewandte Mathematik 92 (1882) 156–171.

[38] R. D. Mindlin, H. Deresiewicz, Elastic Spheres in Contact Under Varying Oblique Forces, Journal of Applied Mechanics 20 (1953) 327–344.

[39] J. J. O'Connor, K. L. Johnson, The role of surface asperities in transmitting tangential forces between metals, Wear 6 (2) (1963) 118–139. doi:10.1016/0043-1648(63)90125-X.

[40] D. Botto, M. Lavella, High temperature tribological study of cobalt-based coatings reinforced with different percentages of alumina, Wear 318 (1-2) (2014) 89–97. doi:10.1016/j.wear.2014.06.024.

[41] M. Lavella, D. Botto, Fretting wear characterization by point contact of nickel superalloy interfaces, Wear 271 (9-10) (2011) 1543–1551. doi:10.1016/j.wear.2011.01.064.
URL http://dx.doi.org/10.1016/j.wear.2011.01.064

[42] C. W. Schwingshackl, E. P. Petrov, D. J. Ewins, Measured and estimated friction interface parameters in a nonlinear dynamic analysis, Mechanical Systems and Signal Processing 28 (2012) 574–584. doi:10.1016/j.ymssp.2011.10.005.
URL http://dx.doi.org/10.1016/j.ymssp.2011.10.005

[43] M. Lavella, Contact Properties and Wear Behaviour of Nickel Based Superalloy René 80, Metals 6 (7) (2016) 159. doi:10.3390/met6070159.
URL www.mdpi.com/journal/metals

[44] S. Fouvry, P. Duó, P. Perruchaut, A quantitative approach of Ti-6Al-4V fretting damage: Friction, wear and crack nucleation, Wear 257 (9-10) (2004) 916–929. doi:10.1016/j.wear.2004.05.011.

[45] S. Toumi, S. Fouvry, M. Salvia, Prediction of sliding speed and normal force effects on friction and wear rate evolution in a dry oscillating-fretting PTFE Ti-6Al-4V contact, Wear 376-377 (2017) 1365–1378. doi:10.1016/j.wear.2017.02.021.
URL http://dx.doi.org/10.1016/j.wear.2017.02.021

[46] B. Van Peteghem, S. Fouvry, J. Petit, Effect of variable normal force and frequency on fretting wear response of Ti-6Al-4V contact, Wear 271 (9-10) (2011) 1535–1542. doi:10.1016/j.wear.2011.01.060.
URL http://dx.doi.org/10.1016/j.wear.2011.01.060

[47] A. L. Mohd Tobi, W. Sun, P. H. Shipway, Evolution of plasticity-based wear damage in gross sliding fretting of a Ti-6Al-4V non-conforming contact, Tribology International 113 (2017) 474–486. doi:10.1016/j.triboint.2017.01.010.

[48] H. Lee, S. Mall, Effect of dissimilar mating materials and contact force on fretting fatigue behavior of Ti-6Al-4V, Tribology International 37 (1) (2004) 35–44. doi:10.1016/S0301-679X(03)00112-9.

[49] A. L. Mohd Tobi, J. Ding, G. Bandak, S. B. Leen, P. H. Shipway, A study on the interaction between fretting wear and cyclic plasticity for Ti-6Al-4V, Wear 267 (2009) 270–282. doi:10.1016/j.wear.2008.12.039.

[50] S. Fouvry, P. Kapsa, L. Vincent, Quantification of fretting damage, Wear 200 (1-2) (1996) 186–205. doi:10.1016/S0043-1648(96)07306-1.

[51] C. Navas, M. Cadenas, J. M. Cuetos, J. de Damborenea, Microstructure and sliding wear behaviour of Tribaloy T-800 coatings deposited by laser cladding, Wear 260 (7-8) (2006) 838–846. doi:10.1016/j.wear.2005.04.020.

[52] C. H. Hager, J. H. Sanders, S. Sharma, Characterization of mixed and gross slip fretting wear regimes in Ti6Al4V interfaces at room temperature, Wear 257 (1-2) (2004) 167–180. doi:10.1016/j.wear.2003.10.023.

[53] X. Huang, R. W. Neu, High-load fretting of Ti-6Al-4V interfaces in point contact, Wear 265 (7-8) (2008) 971–978. doi:10.1016/j.wear.2008.02.018.

[54] Y. Berthier, M. Godet, M. Brendle, Velocity accommodation in friction, Wear 125 (1988) 25–38. doi:10.1080/10402008908981917.

[55] J. Ding, G. Bandak, S. B. Leen, E. J. Williams, P. H. Shipway, Experimental characterisation and numerical simulation of contact evolution effect on fretting crack nucleation for Ti-6Al-4V, Tribology International 42 (2009) 1651–1662. doi:10.1016/j.triboint.2009.04.040.

[56] N. M. Everitt, J. Ding, G. Bandak, P. H. Shipway, S. B. Leen, E. J. Williams, Characterisation of fretting-induced wear debris for Ti-6Al-4 V, Weardoi:10.1016/j.wear.2008.12.032.

[57] M. E. Kartal, D. M. Mulvihill, D. Nowell, D. A. Hills, Determination of the Frictional Properties of Titanium and

22

Nickel Alloys Using the Digital Image Correlation Method, Experimental Mechanics 51 (3) (2011) 359–371. `doi:10.1007/s11340-010-9366-y`.

[58] K. J. Kubiak, T. Liskiewicz, T. Mathia, Surface morphology in engineering applications Inuence of roughness on sliding and wear in dry fretting, Tribology International 44 (2011) 1427–1432.

[59] J. Hintikka, A. Mäntylä, J. Vaara, T. Frondelius, A. Lehtovaara, Stable and unstable friction in fretting contacts, Tribology International 131 (2019) 73–82. `doi:10.1016/j.triboint.2018.10.014`.

[60] J. Juoksukangas, V. Nurmi, J. Hintikka, M. Vippola, A. Lehtovaara, A. Mäntylä, J. Vaara, T. Frondelius, Characterization of cracks formed in large flat-on-flat fretting contact, International Journal of Fatigue 124 (2019) 361–370. `doi:10.1016/j.ijfatigue.2019.03.004`.

[61] C. H. Hager, J. Sanders, S. Sharma, A. Voevodin, Gross slip fretting wear of CrCN, TiAlN, Ni, and CuNiIn coatings on Ti6Al4V interfaces, Wear 263 (1-6 SPEC. ISS.) (2007) 430–443. `doi:10.1016/j.wear.2006.12.085`.

[62] M. R. Hirsch, R. W. Neu, A simple model for friction evolution infretting, Wear 301 (2013) 517–523. `doi:10.1016/j.wear.2013.01.036`.

[63] J. Hintikka, A. Lehtovaara, A. Mäntylä, Fretting-induced friction and wear in large flat-on-flat contact with quenched and tempered steel, Tribology International 92 (2015) 191–202. `doi:10.1016/j.triboint.2015.06.008`.

[64] W. D. Milestone, J. T. Janeczko, Friction between steel surfaces during fretting, Wear 18 (1971) 29–40. `doi:10.1016/0043-1648(71)90062-7`.

[65] I. R. McColl, J. Ding, S. B. Leen, Finite element simulation and experimental validation of fretting wear, Wear 256 (2004) 1114–1127. `doi:10.1016/j.wear.2003.07.001`.

[66] Y. Shen, D. Zhang, S. Ge, Effect of fretting amplitudes on fretting wear behavior of steel wires in coal mines, Mining Science and Technology 20 (2010) 803–808. `doi:10.1016/S1674-5264(09)60285-4`.

[67] P. I. Hurricks, The mechanism of fretting - a review, Wear 15 (1970) 389–409.

[68] D. K. Zhang, S. R. Ge, Y. H. Qiang, Research on the fatigue and fracture behavior due to the fretting wear of steel wire in hoisting rope, Wear 255 (2003) 1233–1237. `doi:10.1016/S0043-1648(03)00161-3`.

[69] T. Yue, M. Abdel Wahab, Finite element analysis of fretting wear under variable coefficient of friction and different contact regimes, Tribology International 107 (2017) 274–282. `doi:10.1016/j.triboint.2016.11.044`.

[70] E. Sauger, S. Fouvry, L. Ponsonnet, P. Kapsa, J. M. Martin, L. Vincent, Tribologically transformed structure in fretting, Wear 245 (2000) 39–52. `doi:10.1016/S0043-1648(00)00464-6`.

[71] S. Fouvry, T. Liskiewicz, P. Kapsa, S. Hannel, E. Sauger, An energy description of wear mechanisms and its applications to oscillating sliding contacts, Wear 255 (1-6) (2003) 287–298. `doi:10.1016/S0043-1648(03)00117-0`.

[72] H. C. Meng, K. C. Ludema, Wear models and predictive equations: their form and content, Wear 181-183 (1995) 443–457.

[73] M. H. Jareland, G. Csaba, Friction Damper Mistuning of a Bladed Disk and Optimization with respect to Wear, in: Proceedings of ASME Turbo Expo 2000, 2000.
URL `http://proceedings.asmedigitalcollection.asme.org`

[74] E. P. Petrov, Analysis of Nonlinear Vibrationd upon Wear-induced Loss of Friction Dampers in Tuned and Mistuned Bladed Discs, in: Proceedings of ASME Turbo Expo 2013: Turbine Technical Conference and Exposition, 2013.
URL `https://proceedings.asmedigitalcollection.asme.org`

[75] L. Salles, L. Blanc, F. Thouverez, A. M. Gouskov, P. Jean, Dynamic Analysis of a Bladed Disk With Friction and Fretting-Wear in Blade Attachments, Proceedings of ASME Turbo Expo 2009: Power for Land, Sea and Air (2009) 465–476`doi:10.1115/GT2009-60151`.
URL `http://proceedings.asmedigitalcollection.asme.org/proceeding.aspx?articleid=1647364`

[76] L. Salles, L. Blanc, F. Thouverez, A. M. Gouskov, Dynamic analysis of fretting-wear in friction contact interfaces, International Journal of Solids and Structures 48 (2011) 1513–1524. `doi:10.1016/j.ijsolstr.2011.01.035`.

[77] J. Armand, L. Pesaresi, L. Salles, C. W. Schwingshackl, A Multi-Scale Approach for Nonlinear Dynamic Response Predictions With Fretting Wear, Journal of Engineering for Gas Turbines and Power 139 (022505) (2017) 1–7. `doi:10.1115/GT2016-56201`.
URL `http://proceedings.asmedigitalcollection.asme.org/proceeding.aspx?doi=10.1115/GT2016-56201`

[78] J. Armand, L. Pesaresi, L. Salles, C. Wong, C. W. Schwingshackl, A modelling approach for the nonlinear dynamics of assembled structures undergoing fretting wear, Proc. R. Soc. A 475 (2223) (2019) 20180731.
URL `http://creativecommons.org/licenses/by/4.0/,whichpermitsunrestricteduse,providedtheoriginalauthorandsourcearecredited`

[79] O. Jin, S. Mall, Effects of independent pad displacement on fretting fatigue behavior of Ti-6Al-4V, Wear 253 (2002) 585–596.

[80] R. S. Magaziner, V. K. Jain, S. Mall, Wear characterization of Ti-6Al-4V under fretting-reciprocating sliding conditions, Wear 264 (2008) 1002–1014. `doi:10.1016/j.wear.2007.08.004`.

[81] S. Fouvry, P. Arnaud, A. Mignot, P. Neubauer, Contact size, frequency and cyclic normal force effects on Ti6Al4V fretting wear processes: An approach combining friction power and contact oxygenation, Tribology International 113 (2017) 460–473. `doi:10.1016/j.triboint.2016.12.049`.

[82] A. Ramalho, J. C. Miranda, The relationship between wear and dissipated energy in sliding systems, Wear 260 (2006) 361–367. `doi:10.1016/j.wear.2005.02.121`.

[83] M. Z. Huq, J. P. Celis, Expressing wear rate in sliding contacts based on dissipated energy, Wear 252 (2002) 375–383. `doi:10.1016/S0043-1648(01)00867-5`.

[84] B. D. Leonard, Head of the Graduate Program Date An Experimental and Numerical Investigation of the Effect of Coatings and the Third Body on Fretting Wear Doctor of Philosophy, Ph.D. thesis, Purdue University (2012).
URL `http://www.purdue.edu/policies/pages/teach{_}res{_}outreach/c{_}22.html`

[85] V. Done, D. Kesavan, M. Krishna R, T. Chaise, D. Nelias, Semi analytical fretting wear simulation including wear debris,

Tribology International 109 (2017) 1–9. `arXiv:15334406`, `doi:10.1016/j.triboint.2016.12.012`.

[86] S. R. Pearson, P. H. Shipway, Is the wear coefficient dependent upon slip amplitude in fretting? Vingsbo and Söderberg revisited, Wear (330-331) (2015) 93–102. `doi:10.1016/j.wear.2014.11.005`.

[87] S. D. Stearns, N. Ahmed, Digital signal analysis, IEEE Transactions on Systems, Man, and Cybernetics (10) (1976) 724.

[88] M. Feldman, Hilbert transform applications in mechanical vibration, John Wiley & Sons, 2011.

[89] H. Sumali, R. Kellogg, Calculating damping from ring-down using hilbert transform and curve fitting, in: 4th International Operational Modal Analysis Conference, IOMAC 2011, 2011. `doi:10.5285/78114093-E2BD-4601-8AE5-3551E62AEF2B`.

[90] M. W. Sracic, M. S. Allen, H. Sumali, Identifying the Modal Properties of Nonlinear Structures Using Measured Free Response Time Histories from a Scanning Laser Doppler Vibrometer, in: 30th International Modal Analysis Conference (IMAC XXX), Jacksonville, FL, 2012.

[91] M. Jin, M. R. W. Brake, H. Song, Comparison of Nonlinear System Identification Methods for Free Decay Measurements with Application to Jointed Structures, Journal of Sound and Vibration Accepted.

[92] K. J. Moore, M. Kurt, M. Eriten, D. M. McFarland, L. A. Bergman, A. F. Vakakis, Wavelet-bounded empirical mode decomposition for measured time series analysis, Mechanical Systems and Signal Processing 99 (2018) 14–29. `doi:10.1016/j.ymssp.2017.06.005`.

[93] K. Guo, X. Zhang, H. Li, H. Hua, G. Meng, A New Dynamical Friction Model, International Journal of Modern Physics B 22 (08) (2008) 967–980. `doi:10.1142/S0217979208039010`.
URL `http://www.worldscientific.com/doi/abs/10.1142/S0217979208039010`

[94] F. Ma, H. Zhang, A. Bockstedte, G. C. Foliente, P. Paevere, Parameter Analysis of the Differential Model of Hysteresis, Journal of Applied Mechanics 71 (3) (2004) 342. `doi:10.1115/1.1668082`.
URL `http://appliedmechanics.asmedigitalcollection.asme.org/article.aspx?articleid=1415149`

[95] M. Brake, An Overview of Constitutive Models, in: M. R. W. Brake (Ed.), The Mechanics of Jointed Structures, Springer International Publishing, Cham, 2018, pp. 207–221. `doi:10.1007/978-3-319-56818-8_14`.
URL `https://doi.org/10.1007/978-3-319-56818-8{_}14`

[96] M. Ismail, F. Ikhouane, J. Rodellar, The hysteresis Bouc-Wen model, a survey, Archives of Computational Methods in Engineering 16 (2) (2009) 161–188. `doi:10.1007/s11831-009-9031-8`.

RESEARCH HIGHLIGHTS

- The impact of wear on the dynamics of structures has been experimentally quantified
- Wear leads to shifts in natural frequency and damping of structure vibration modes
- Wear needs to be included in models to capture the dynamics of jointed structures
- A Bouc-Wen formulation is presented to account for wear in dynamic simulations